Rundong Zhang

Department of Mechanical and Aerospace Engineering, The Ohio State University, Columbus, OH 43210 e-mail: zhang.10083@osu.edu

Shuai Wu

Department of Mechanical and Aerospace Engineering, The Ohio State University, Columbus, OH 43210 e-mail: wu.4309@osu.edu

Qiji Ze

Department of Mechanical and Aerospace Engineering, The Ohio State University, Columbus, OH 43210 e-mail: ze.3@osu.edu

Ruike Zhao

Department of Mechanical and Aerospace Engineering, The Ohio State University, Columbus, OH 43210 e-mail: zhao.2885@osu.edu

Micromechanics Study on Actuation Efficiency of Hard-Magnetic Soft Active Materials

Hard-magnetic soft active materials have drawn significant research interest in recent years due to their advantages of untethered, rapid and reversible actuation, and large shape change. These materials are typically fabricated by embedding hard-magnetic particles in a soft matrix. Since the actuation is achieved by transferring the microtorques generated on the magnetic particles by the applied magnetic field to the soft matrix, the actuation depends on the interactions between the magnetic particles and the soft matrix. In this paper, we investigate how such interactions can affect the actuation efficiency by using a micromechanics approach through the representative volume element simulations. The micromechanics reveals that particle rotations play an essential role in determining the actuation efficiency, i.e., the torque transmission efficiency. In particular, a larger local particle rotation in the matrix would reduce the effective actuation efficiency. Micromechanics simulations further show that the efficiency of the torque transmission from the particles to the matrix depends on the particle volume fraction, the matrix modulus, the applied magnetic field strength, as well as the particle shape. Based on the micromechanics simulations, a simple theoretical model is developed to correlate the torque transmission efficiency with the particle volume fraction, the matrix modulus, as well as the applied magnetic field strength. We anticipate this study on the actuation efficiency of hardmagnetic soft active materials would provide optimization and design guidance to the parameter determination for the material fabrication for different applications. [DOI: 10.1115/1.4047291]

Keywords: magnetic soft materials, soft active materials, stimuli-responsive materials, micromechanics, soft robotics, computational mechanics, constitutive modeling of

1 Introduction

Hard-magnetic soft active materials (hmSAMs) are a type of stimuli-responsive materials that has attracted significant research interests in recent years due to their advantages of untethered, rapid, and reversible actuation, as well as large shape changes with the potential for applications including soft robotics [1-5], active metamaterials [2,6-10], and biomedical devices [11-17]. hmSAMs are fabricated by embedding micrometer-sized highremanence, high-coercivity magnetic particles, such as NdFeB, into a soft matrix [2,5]. Figure 1(a) schematically shows the actuation mechanism of hmSAMs. After solidifying the soft composite, the hard-magnetic particles in the soft matrix can be magnetized along desired directions (such as the horizontal direction in Fig. 1(a)) under a large impulse magnetic field (~ 1.5 T). The high remanence of hard-magnetic particles allows them to retain a strong magnetic moment density, also called magnetization (M). Upon the application of a small magnetic field (typically < 200 mT, much less than the coercivity of the magnetic particle) whose direction is not along the hmSAM's magnetization direction (such as the vertical direction in Fig. 1(b)), microtorques are generated to rotate the particles so that their magnetic polarities tend to align with the applied field [7,18-20]. Assuming perfect bonding between the particles and matrix, the microtorques transmit to the soft matrix and the entire hmSAM bends, leading to large deformation and shape change of the hmSAM under the magnetic actuation (Fig. 1(b)). Since the generation of microtorques is instantaneous

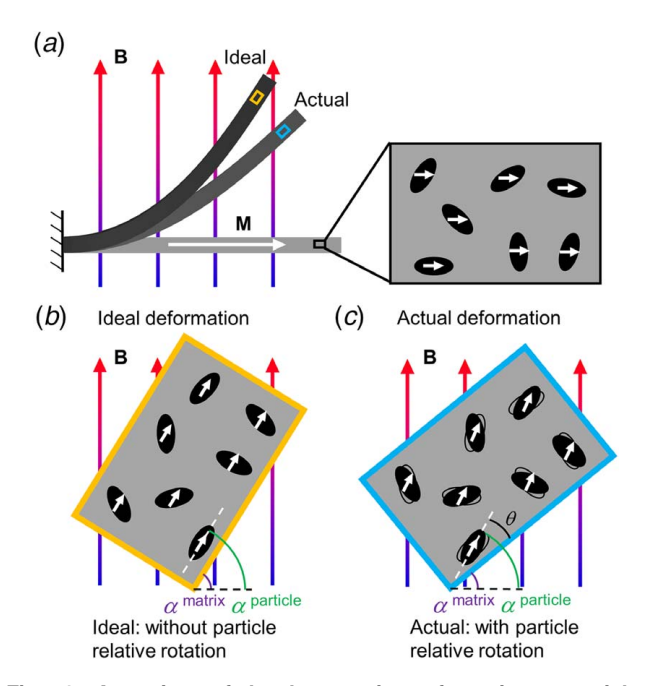


Fig. 1 Actuation of hard-magnetic soft active materials: (a) mechanism of the magnetic actuation of a beam bending, (b) schematics of the actuation with the ideal torque transmission, and (c) schematics of the actuation with reduced torque transmission efficiency due to particle's local rotation in the soft matrix. The black line profiles denote the particle orientations if there were no particle local rotations with respect to the matrix.

materials, mechanical properties of materials

¹Corresponding author.

Manuscript received April 29, 2020; final manuscript received May 18, 2020; published online June 9, 2020. Assoc. Editor: Shaoxing Qu.

and the matrix is rubber-like, hmSAMs exhibit rapid and reversible actuation. This also permits complicated actuation patterns by controlling local magnetization directions within hmSAMs, making them attractive for a wide range of applications [1,7,21].

The mechanics of general magnetoactive materials has been studied intensively in the past, with a strong focus on magnetorheological elastomers and ferrogels [22-26], where soft-magnetic particles such iron and iron oxide are used as fillers in a soft matrix. For these material composites, the magnetic particles cannot provide magnetic torque as their magnetization always follows the external applied magnetic field; thus, no particle rotation is induced by the magnetic field. For hmSAMs with the particles' microtorques as the driving force for actuation, mechanics studies have just emerged. Zhao et al. recently developed a continuum-level nonlinear field theory to describe the finite mechanical deformation of the hmSAM under the applied magnetic field [19]. This model has been shown to effectively capture the magneto-mechanical behaviors of hmSAMs. However, the existing models treat the hmSAM as a continuum homogeneous solid, where the actuation force, or the magnetic torque, is quantified by the magnetization of the hmSAM in its bulk form and the strength of the applied field. This homogenization model considers the magnetic actuation similar to an external mechanical loading, whereas the actual magnetic actuation mechanism is based on the microscale interaction between the magnetic particles and the soft matrix, due to the discrete microtorques acting on the particles upon the application of a magnetic field. The induced microtorques transmit to the soft matrix, which further drives the whole composite to deform. The transmission efficiency of these microtorques to the surrounding matrix can be significantly affected by the particle spatial distribution, particleparticle interaction, and the particle-matrix interaction caused by the property mismatches at the interfaces. Intuitively, to facilitate actuation with large deformation and shape change under a relatively small magnetic field, the matrix should be relatively soft to reduce the material's resistance to deforming. However, to achieve the ideal transmission of microtorques, the matrix should be stiff enough such that the local particle rotation with respect to the surrounding matrix could be minimized. In this case, a soft matrix is not an ideal choice as it permits the local rotation of the particle within the matrix and reduces the torque transmission efficiency. As shown in Fig. 1(b), assuming no relative deformation at the particle–matrix interface, the matrix rotates together with the magnetic particles and the torque is transmitted 100% to the matrix, and the angle of absolute rotation for the matrix is the same as the angle of absolute rotation of the particle (α matrix = α particle). However, if the matrix is soft enough to allow relative deformation at the particle-matrix interface (Fig. 1(c)), the magnetic torques acting on the particles fail to be completely transmitted to the soft matrix. Instead, part of the torque results in the elastic distortion around the particles, which is denoted by the particle rotation θ with respect to the matrix. In this case, the absolute angle of rotation for the matrix is smaller than the absolute angle of rotation of the particle (α matrix < α particle). Therefore, to precisely evaluate the effective torque transmitted to the matrix and accurately predict the deformation of hmSAMs under magnetic actuation, a systematic micromechanics study of the actuation mechanism is of crucial importance but is currently lacking.

This paper aims to study the micro-mechanism of the magnetic actuation by investigating the torque transmission efficiency of the magnetic particles in hmSAMs. A computational micromechanics approach is first introduced by integrating representative volume element (RVE) models with a user-defined element (UEL) subroutine based on the constitutive model recently developed for hmSAMs [19] to investigate how matrix modulus, particle volume fraction, particle shape, and particle–particle and particle–matrix interactions can affect the torque transmission efficiency. Based on the simulation results from the RVE models, a homogenization model is developed to consider the torque transmission efficiency obtained from the micro-mechanism study of the magnetic actuation. This new homogenization model can be used to guide

the parameter determination of hmSAM fabrication for different applications.

2 Methods

2.1 Constitutive Model for hmSAMs. In this paper, the continuum-level constitutive model developed by Zhao et al. [19] is employed to capture the mechanical deformation of hmSAMs under an applied magnetic field. This model is briefly described as follows.

Under the continuum mechanics framework, we consider an hmSAM placed in a magnetic field. A material point \mathbf{X} in the undeformed configuration (or the reference configuration) moves to \mathbf{x} in the current configuration through a deformation gradient $\mathbf{F} = d\mathbf{x}/d\mathbf{X}$ due to applied mechanical forces and magnetic fields. We denote vector \mathbf{B} as the applied magnetic flux density (or magnetic field for convenience) in the current configuration. The magnetic field can be generated by a pair of electromagnetic coils in the air. Correspondingly, the nominal applied magnetic field in the reference configuration is denoted by $\hat{\mathbf{B}}$. The relationship between \mathbf{B} and $\hat{\mathbf{B}}$ is

$$\tilde{\mathbf{B}} = J\mathbf{F}^{-1}\mathbf{B} \tag{1}$$

where J denotes the deformation Jacobian ($J = \det \mathbf{F}$). The hmSAM has an initial magnetization of \mathbf{M} in the current configuration and $\tilde{\mathbf{M}}$ in the reference configuration. Note that the permeability of the magnetized hard-magnetic particles is regarded to be the air/vacuum permeability, and the magnetic field \mathbf{B} inside the hmSAM would be the same as it is in the air. Applying the magnetic field \mathbf{B} tends to align \mathbf{M} in the \mathbf{B} direction, which changes the magnetic potential of the hmSAM by [27]

$$W^{\text{magnetic}} = -\mathbf{M} \cdot \mathbf{B}, \quad \text{or} \quad \tilde{W}^{\text{magnetic}} = -\mathbf{F}\tilde{\mathbf{M}} \cdot \mathbf{B}$$
 (2)

Then, the total Helmholtz free energy of the hmSAM per unit volume in the reference configuration can be expressed as

$$\tilde{W} = \tilde{W}^{\text{elastic}}(\mathbf{F}) - \mathbf{F}\tilde{\mathbf{M}} \cdot \mathbf{B} \tag{3}$$

We further obtain the Cauchy stress as

$$\sigma = \frac{1}{J} \frac{\partial \tilde{W}^{elastic}(\mathbf{F})}{\partial \mathbf{F}} \mathbf{F}^{T} - \frac{1}{J} \mathbf{B} \otimes \mathbf{F} \tilde{\mathbf{M}} = \frac{1}{J} \frac{\partial \tilde{W}^{elastic}(\mathbf{F})}{\partial \mathbf{F}} \mathbf{F}^{T} - \mathbf{B} \otimes \mathbf{M}$$
(4)

The body torque \mathbf{m} generated by the magnetized domain under the action of the applied magnetic field is derived as

$$\mathbf{m} = \mathbf{M} \times \mathbf{B} \tag{5}$$

This model has been implemented into a user element subroutine (UEL) in commercial finite element simulation package ABAQUS (Dassault Systemes, Vélizy-Villacoublay, France). The UEL is used in the finite element (FE) simulations in this paper.

2.2 Representative Volume **Elements.** Representative volume elements are frequently used to study the mechanics of composite materials [28-30]. Many tools and algorithms are developed to generate different kinds of RVEs to address engineering problems [31-34]. In this work, we investigate the micromechanism of the magnetic actuation and study the magnetic particle's torque transmission efficiency using RVE models in FE simulations. We start our RVE model from using circular particles considering the random shapes and orientations of the particles that are distributed in the matrix, as shown in the scanning electron microscopic (SEM) images in Fig. 2(a). In this paper, we utilize two-dimensional RVE models to reveal the insight into how the particle's torque transmission efficiency would be affected by the dominating factors including particle volume fraction, particle-matrix modulus ratio, and the magnetic field, but the insight from the 2D RVE studies can be extended to the general 3D problems. Note

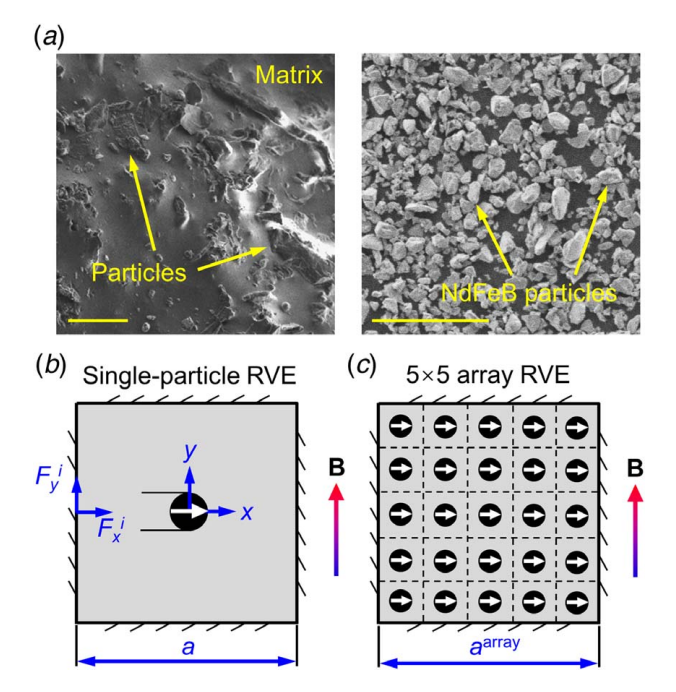


Fig. 2 RVE models of hmSAMs: (a) SEM images of NdFeB particles in a soft matrix and NdFeB particles only. The scale bars are $50\,\mu\text{m}$. (b) A single-particle RVE model for a low particle volume fraction case and (c) a high particle volume fraction RVE model with a 5×5 particle array.

that three-dimensional RVE models will be required to consider the contribution of the out-of-plane dimension [35,36], which is not the focus of this paper but will be investigated in the future. Figure 2(b)shows an RVE with a single hard-magnetic particle at the center of a square matrix. For cases with low particle volume fraction, the single-particle RVE model can be used to effectively investigate the torque transmission and the mechanical behavior in the matrix as the influence from surrounding particles is negligible due to far particle-to-particle distance. Note that the hmSAMs with low particle volume fractions are usually used for applications with lowstiffness and low-density considerations. Here, we look at the shear strain along the matrix edges to determine the critical particle volume fraction f, below which we can use single-particle RVEs to study the micromechanics of hmSAMs. By constraining the edge shear strain to be less than 10% of the maximum shear strain at the particle-matrix interface when B = 100 mT, we consider $f \le$ 5% as low particle volume fraction.

In all single-particle RVE simulations, we fix the size of the unit cells and change the diameters of the particle to obtain different volume fractions. For a given volume fraction f, the diameter D of the magnetic particle can be derived as

$$D = 2a\sqrt{\frac{f}{\pi}} \tag{6}$$

where a is the side length of the square unit cell. The matrix is modeled as a neo-Hookean solid with a shear modulus ranging from 10 kPa to 50 kPa, which is typical in hmSAMs. The magnetic particle is modeled using the above-discussed hmSAM constitutive model with a shear modulus of $G_p = 300$ MPa. It is worth mentioning that although the modulus for particle does not reflect the real particle modulus (shear modulus \sim 65 GPa), it is sufficiently high to mimic an almost rigid material comparing to the matrix and in the meantime minimizing the convergence issues in the simulations. The magnetization of the particle is along the horizontal direction with M = 600 kA/m, a constant throughout this study. Note that the magnetization constant can vary based on the NdFeB particle size and manufacturing methods [37,38]. Here,

we choose M = 600 kA/m, which is within the common range of magnetization of NdFeB particles that are around 5 μ m. As shown in Fig. 2(b), the applied magnetic field is along the vertical direction, perpendicular to the particle's magnetization. Fixed boundary conditions are applied to all four edges of the matrix square. To calculate the transmitted torque in the matrix, the reaction forces on the nodes on the sides of the square matrix are obtained from the FE simulations, with F_x^i and F_y^i being the reaction forces in the x-direction and y-direction of the ith node, respectively. The resultant total torque is calculated as

$$T_{\text{tot}} = \Sigma_i (F_x^i y^i - F_y^i x^i) \tag{7}$$

where x^i and y^i are the x- and y-direction coordinates of the ith node. The origin of the coordinate system is set at the center of the particle.

Note that for the cases with larger particle volume fraction, the single-particle RVE model is no longer accurate to describe the torque transmission and the deformation in the matrix, as the torque induced by adjacent magnetic particles would also contribute to the matrix deformation [39,40]. To consider the effect of particleparticle interaction on matrix behavior, RVE models with an array of particles are used to evaluate the effective torque transmission, as shown in Fig. 2(c). Here, a 5×5 particle array RVE model is used for high particle volume fraction simulations as it could accurately represent the large material area with moderate computation time. To show that the 5×5 array RVE model can be used to correctly estimate the mechanical behavior of the particles in the soft matrix, we compare the results with other those of array models (see Supplemental Fig. 1 available in the Supplemental Materials on the ASME Digital Collection). In the 5×5 RVE model, the four boundaries of the square with length $a^{array} = 5a$ are fixed the same way as in the single-particle RVE model. The reaction forces on the nodes and the resultant total torque can be derived following the method for the single-particle RVE model (Eq. (7)).

2.3 Torque Transmission Efficiency. To quantify how efficiently the torque can be transmitted from the particle to the matrix, we introduce a parameter, the torque transmission efficiency η , defined as the ratio between the total reaction torque from the matrix and the total torque induced by the magnetic particles. In the case shown in Fig. 1(a), the total torque induced by the magnetic field on the magnetic particles is calculated as

$$m_{\text{tot}} = MBV_p = MBa^2 f \tag{8}$$

where V_p is the volume of the magnetic particles. The torque transmission efficiency η is then derived as

$$\eta = \frac{T_{\text{tot}}}{m_{\text{tot}}} \tag{9}$$

where T_{tot} is calculated from the FE simulation results using Eq. (7).

3 Results and Discussions

3.1 Low Particle Volume Fraction. We first study the case with a low particle volume fraction of 2% and matrix shear modulus G = 20 kPa. At this volume fraction, particles are far away from each other and the particle–particle interaction is negligible. Therefore, the single-particle RVE model can be adopted to investigate the mechanical response of the matrix due to the magnetic torque acting on an individual particle.

Figure 3(a) shows the contour plots of the shear strain γ_{xy} at different applied magnetic fields. As the magnetic field B increases from 20 mT to 120 mT, the particle intends to align its magnetization with the applied field and rotates counterclockwise from θ = 0.14 (or 8 deg) at 20 mT to θ = 0.66 (or 38 deg) at 120 mT. Figure 3(b) shows the particle rotation angle increases slightly nonlinearly with the applied magnetic field. The rotation introduces

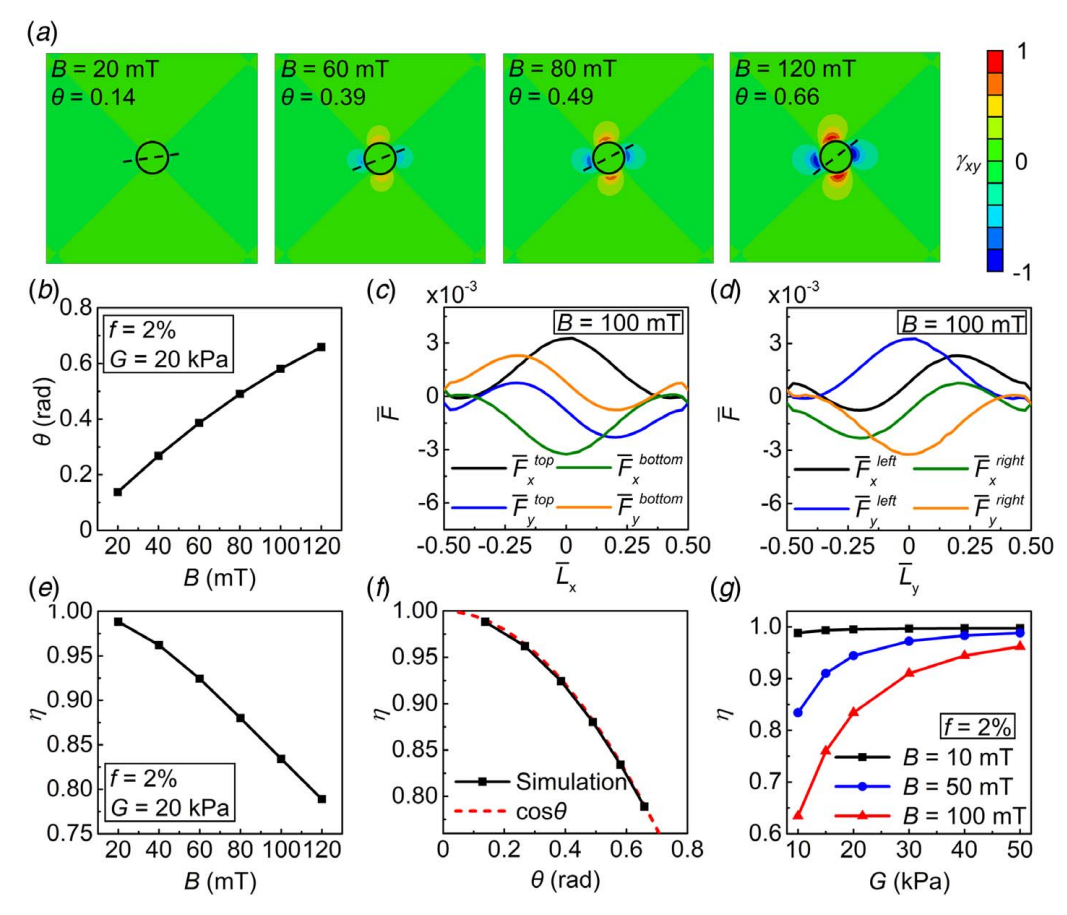


Fig. 3 Results from the low particle volume fraction RVE model: (a) shear strain contours showing particle rotation in the matrix under different magnetic field strengths for the hmSAM with 20 kPa matrix shear modulus and 2% particle volume fraction, (b) particle rotation angle as a function of the applied magnetic field, (c) distribution of the reaction forces on the top and bottom edges of the matrix at B=100 mT, (d) distribution of the reaction forces on the left and right edges of the matrix at B=100 mT, (e) torque transmission efficiency as a function of the applied magnetic field, (f) torque transmission efficiency as a function of the particle rotation angle and the fitting curve $\cos \theta$, and (g) torque transmission efficiency as a function of the shear modulus of the soft matrix at different applied magnetic fields.

shear strain around the particle, and the maximum shear strain occurs at the interface between the particle and the matrix. The shear strain decays rapidly when measured away from the particle. For the case with the largest magnetic field applied (120 mT), the shear strain decreases 90% at roughly about one particle diameter away from the particle edge. Although the shear strain around the particle increases with the increasing magnetic field, its maximum value along the edges of the matrix decays to the negligible 4.7% the shear strain around the particle at B=120 mT, further demonstrating that the single-particle RVE model is sufficient to describe the mechanical behavior of the hmSAM with 2% particle volume fraction

Figures 3(c) and 3(d) show the distribution of the reaction forces on the top and bottom sides and the left and right sides, respectively, with B=100 mT. The reaction forces and the x- (or y-) direction coordinate are normalized as $\bar{F}_i = F_i D/m_{\rm tot}(i=x,{\rm or}\ y)$ and $\bar{L}_x = x/a$ (or $\bar{L}_y = y/a$), respectively. For the top and bottom sides (Fig. 3(c)), the x-direction reaction forces, which are shear forces, indicate mirror symmetry with respect to the y-axis at $\bar{L}_x = 0$. The shear forces also reach their maximums at the center of the sides ($\bar{L}_x = 0$). The y-direction forces, which are normal forces perpendicular to the sides, demonstrate twofold skew-symmetry: they are skew-symmetric with respect to the y-axis at $\bar{L}_x = 0$. The distributions of the reaction forces on the top and bottom sides confirm that they all contribute to the total torque of the RVE. For the reaction forces on the left and right sides, they exhibit similar features as those on the top and bottom sides. It

should be noted that these reaction force distributions, which exhibit the torsional behavior, drive the overall deformation of the hmSAM.

Figure 3(e) shows the torque transmission efficiency as a function of the applied magnetic field. It can be seen that as the applied field increases, the torque transmission efficiency decreases. This is because a larger magnetic field leads to a larger particle rotation in the matrix. As the particle rotates, the torque generated by the applied magnetic field decreases, as shown by Eq. (5). As the particle rotates, its magnetization M rotates with the particle, leading to

$$m_p = MB\cos\theta \tag{10}$$

where m_p is the torque generated on the particle. This observation is confirmed by Fig. 3(f), which shows the torque transmission efficiency as a function of the particle rotation angle θ , perfectly fitted by the $\cos\theta$ function, as indicated by the dashed line. Therefore, to obtain a high torque transmission efficiency, a relatively stiff matrix is preferred to minimize the particle's local rotation. This is further confirmed by Fig. 3(g), in which the torque transmission efficiency is plotted as functions of the shear modulus of the matrix at different applied magnetic fields. Under a small magnetic field, such as B=10 mT, the torque transmission efficiency decreases slightly as the shear modulus is reduced. But when B is increased, the torque transmission efficiency drops significantly for the soft matrix. For example, under B=100 mT, when the shear modulus of the matrix is 10 kPa, torque transmission

efficiency drops to \sim 0.63. When the shear modulus of the matrix is 50 kPa, larger than 0.98 torque transmission efficiency can be obtained under the applied magnetic field that is smaller than 100 mT. As a result from the single-particle RVE model, the increase in applied magnetic field and decrease in the shear modulus of matrix both contribute to the decrease in the torque transmission efficiency.

3.2 High Particle Volume Fraction. When the particle volume fraction is low, single-particle RVE model is sufficient to describe the mechanical behavior of the composite and calculate the torque transmission efficiency, as particles are far away from each other and thus do not interact. When the particle loading becomes higher, the particles are closer to each other and their mechanical responses will interfere with each other; thus, the matrix deformation around particles will be affected by the particle–particle interaction [39–42]. To investigate how the particle–particle and particle–matrix interactions can affect the torque transmission efficiency, we conduct FE simulations using the 5×5 particle array RVE model as previously described in Fig. 2(c).

Figure 4(a) shows the result with a 15% volume fraction of particles and shear modulus of 20 kPa at B = 100 mT. At 15% volume fraction, the shear strain measured between two adjacent particles and away from each particle does not decay to zero, indicating particle–particle interaction. The zoomed-in contour plot of the shear strain distribution between two adjacent particles for four cases, 2%, 5%, 15%, and 25%, is shown in Fig. 4(b). The contour plots clearly demonstrate that the shear strain between two adjacent particles increases as the particle loading increases. To quantitatively investigate particle–particle interaction, the dotted line in Fig. 4(c)

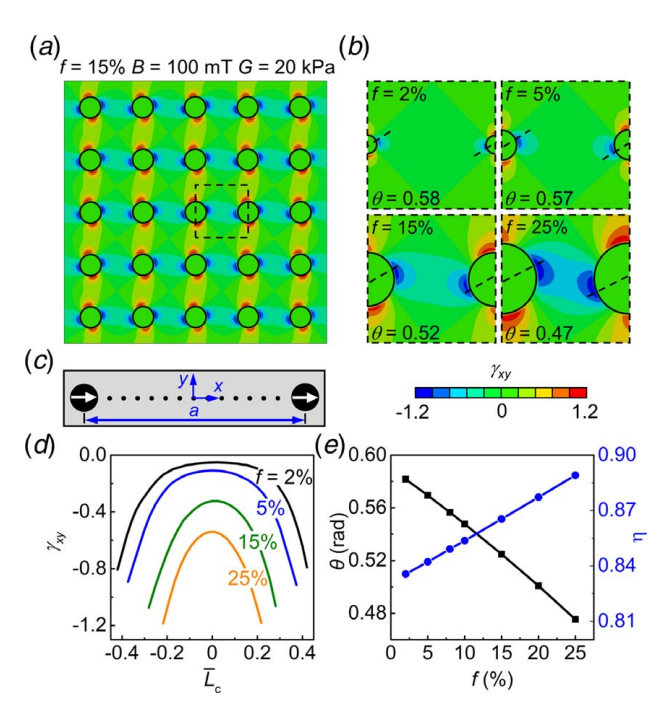


Fig. 4 Results of high particle volume fraction RVE models under $B=100\,\mathrm{mT}$ and $G=20\,\mathrm{kPa}$: (a) contour plot of the shear strain distribution for a 5×5 array model for 15% particle volume fraction; (b) zoomed-in shear strain distribution for RVE models with different particle volume fractions. The zoomed-in area is marked by a black dashed rectangle in (a). (c, d) schematics and results of the matrix shear strain measurement between two adjacent particles for different particle volume fractions. (e) Particle rotation (solid curve with diamond dots) and torque transmission efficiency (solid curve with rounded dots) as functions of the particle volume fraction.

shows the schematics of the shear strain measurement taken between the two adjacent particles, along the horizontal direction at the undeformed configuration. The x-direction coordinate of the measured point is normalized as $\bar{L}_c = x/a$, with the origin located at the midpoint between two adjacent particles. Figure 4(d) shows the corresponding shear strain distribution between two adjacent particles for the four different particle volume fractions. As particle loading increases, the overall magnitude of the shear strain increases significantly; i.e., both the maximum shear strain at the particle-matrix interface and the shear strain between two adjacent particles increase. However, with the increasing shear strain, particle rotation angle decreases, as shown in Fig. 4(e). This is opposite to the low particle volume fraction case, where the particle interaction does not exist, and the increase in particle rotation angle increases the magnitude of the shear strain (Fig. 3(a)). Such a difference clearly indicates that a strong interaction between particles would develop as the particle loading increases. As a result, the particle-particle interaction restrains the particle's local rotation, which increases the overall torque transmission efficiency of the material, as shown by the solid curve with rounded dots in Fig. 4(e). Consequentially, the increase in particle volume fraction leads to the increase in the torque transmission efficiency.

3.3 Effects of Particle Shape on Magnetic Actuation. As real particles have different shapes, especially for particles with an average shape and aspect ratio, it is also necessary to consider the effects of particle shape on actuation efficiency. Here, we consider particles of rectangular shape with aspect ratios w/h = 1, 2, and 3, where w is the particle width and h is the particle height, as defined in Fig. 5(a). We conduct FE simulations for both the singleparticle RVEs and the array-particle RVEs for hmSAMs with the matrix shear modulus of 20 kPa. Figure 5(a) shows the results of the single-particle RVE models on the shear strain contours of different particle shapes with the particle volume fraction of 2% under B = 100 mT. Here, in order to reduce stress/strain concentration at the corners for the rectangular particles, the corners are rounded with a radius of 1/40 a (see Supplemental Figs. 2 and 3 available in the Supplemental Materials on the ASME Digital Collection). As seen from the shear strain contour plots, even with rounded corners, the shear strain near the corners are still very high. Figure 5(b) shows the particle rotation angle as a function of the magnetic field for particles with different shapes, i.e., the circular shape and the rectangular shape with different aspect ratios. As can be seen, although a larger magnetic field leads to high particle rotation in general, the higher aspect ratio of rectangular particles constrains the particle rotation significantly. For example, at B = 100 mT, the rotation angle changes from θ = 0.58 (or 33 deg) for the circular particles to $\theta = 0.38$ (or 22 deg) for the rectangular particles with the aspect ratio of 3.

We further investigate the effects of particle shape at high particle volume fraction. Figure 5(c) shows the shear strain contours for the cases with different particle shapes at a particle volume fraction of 15% under B = 100 mT. For the systems with different particle shapes but the same particle volume fraction, the gap between two adjacent particles in the particle's long axis direction is smaller for the case with a higher aspect ratio than it is for a lower aspect ratio one. The smaller gap would induce larger particle-particle interaction and then constrains the particle rotation more. Figure 5(d) shows the particle rotation angle as a function of particle volume fraction for particles with different shapes. At 15% particle volume fraction, the rotation angle drops from θ = 0.52 (or 30 deg) for circular particles to $\theta = 0.31$ (or 18 deg) for rectangular particles with aspect ratio of 3. Figure 5(e) shows the torque transmission efficiency as a function of particle volume fraction under B = 100 mT for particles with different shapes, where it conclusively indicates that higher particle volume fraction and larger particle aspect ratio would lead to higher torque transmission efficiency. It should be noted that although the particle shape plays a significant role in determining the torque transmission efficiency,

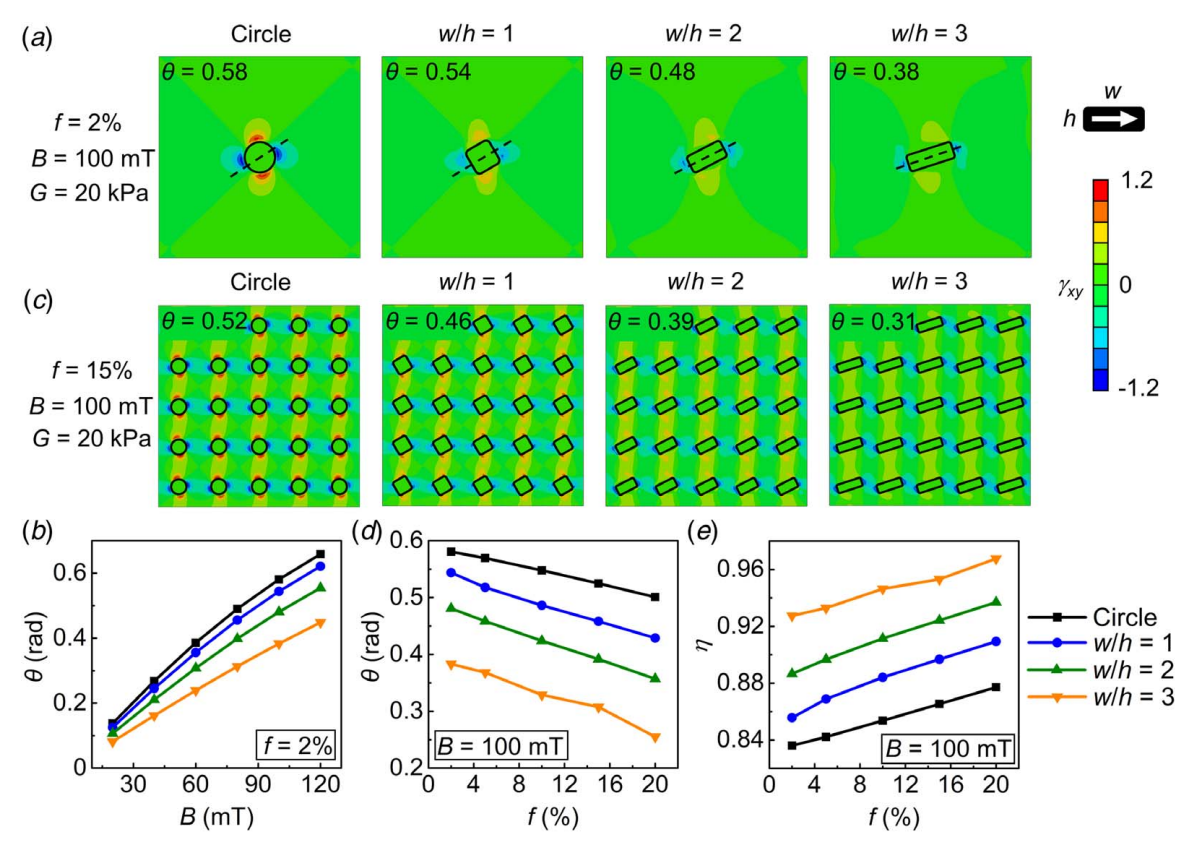


Fig. 5 Effects of particle shape on magnetic actuation of hmSAMs with the matrix shear modulus of 20 kPa: (a) contour plots of shear strain for single-particle RVEs with different particle shapes, (b) particle rotation as a function of the applied magnetic field for different particle shapes, (c) contour plots of shear strain for array-particle RVEs with different particle shapes, and (d, e) particle rotation and torque transmission efficiency as functions of particle volume fraction for different particle shapes under B = 100 mT

the general trend and the insight obtained from circular shaped particles are the same as those from the rectangular particles. For hmSAMs, the hard-magnetic particles have size and shape distributions, which could be analyzed via the statistical approach together with the current RVE methods to determine the effective torque transmission efficiency.

3.4 A Homogenized Model for Torque Transmission Efficiency. Based on the understandings obtained from RVE simulations, we develop a simple homogenized model to describe how the torque transmission efficiency depends on the particle volume fraction, the matrix shear modulus, as well as the applied magnetic field (see Supplementary Materials for details). We start with considering a simplified problem, as shown in Fig. 6(a) where a rigid circular particle is embedded in a circular matrix. R_1 and R_2 denote the radius of the particle and the matrix, respectively. The matrix is fixed at the outside boundary. An applied magnetic field rotates the particle by (see Supplementary Materials for details)

$$\theta = \frac{MB}{2G}(1 - f) \tag{11}$$

By considering the geometry difference between the RVE and the model developed above (Fig. 6(a)) as well as the upper bound of particle rotation to be $\pi/2$, the above equation can be modified as (see Supplementary Materials for details)

$$\theta = \frac{\pi}{2} \left(1 - \frac{\pi}{4} f \right) \left[1 - \exp\left(\frac{kMB}{G}\right) \right]$$
 (12)

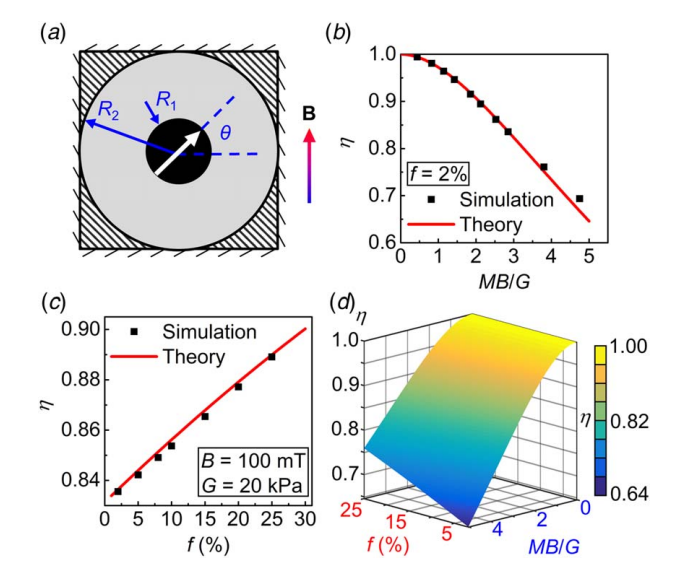


Fig. 6 Homogenization model of the torque transmission efficiency for hmSAMs: (a) schematics of the simplified particlematrix model, (b, c) theoretical fitting of the simulation results on the torque transmission efficiency as functions of (b) the normalized magnetic field and (c) the particle volume fraction, and (d) the parameter design space for the normalized magnetic field and the particle volume fraction.

where k is a fitting coefficient. By fitting Eq. (12) with the RVE results on the particle rotation angle, we obtain k = -0.165. Therefore, we have the torque transmission efficiency at

$$\eta = \cos \theta = \cos \left\{ \frac{\pi}{2} \left(1 - \frac{\pi}{4} f \right) \left[1 - \exp \left(-0.165 \frac{MB}{G} \right) \right] \right\}$$
 (13)

Figure 6(b) compares the theoretical and simulation results of the torque transmission efficiency as a function of the normalized magnetic field MB/G for the low volume fraction case (2%), based on Eq. (13). The developed theory can accurately describe the simulation observation for a wide range of the normalized magnetic field. It is worth mentioning that the fitted theoretical prediction of the magnetic actuation of hmSAMs is even valid for large deformation cases. To give a scaling example, when MB/G = 4 with the magnetization M = 600 kA/m (a typical number for NdFeB particles) and G = 15 kPa (a typical number for soft materials such as Ecoflex and gels), the applied magnetic field will be B = 100 mT, which can lead to significantly large deformation. Figure 6(c) shows the theoretical result of the torque transmission efficiency as a function of the particle volume fraction. Again, the theory matches very well with the RVE simulations. It can be seen that the torque transmission efficiency increases linearly with the particle loading of the hmSAM. After validating the correctness and accuracy of the developed theoretical model, we systematically plot the torque transmission efficiency in the parameter design space for the normalized magnetic field and the particle volume fraction based on Eq. (13), as shown in Fig. 6(d), which summarizes the methods of increasing the torque transmission efficiency. In general, increasing the particle volume fraction and using a relatively stiff matrix can facilitate the increase in the torque transmission efficiency. We anticipate this diagram would provide design guidance for the material parameter determination of hmSAM for desired applications.

4 Conclusion

The micromechanics of torque transmission from magnetic particles to the hard-magnetic soft active material is studied in this paper. Representative volume element models are first built to study the effect of the particle volume fraction, the matrix shear modulus, the applied magnetic field, and the particle shape. A theoretical model is also developed. It is found that the torque transmission efficiency is determined by the particle rotations. Mechanisms such as higher particle volume fractions, a stiffer matrix, and particles with high aspect ratios can prevent particle rotation in the matrix, and thus would help increase the torque transmission efficiency. The insight obtained from this study can guide the design of hard-magnetic soft active materials with higher actuation efficiency.

Conflict of Interest

There are no conflicts of interest.

Data Availability Statement

The data sets generated and supporting the findings of this article are obtainable from the corresponding author upon reasonable request. The authors attest that all data for this study are included in the paper. Data provided by a third party are listed in Acknowledgement.

Acknowledgment

The authors acknowledge the support from the NSF Award (CMMI-1939543) and the NSF Career Award (CMMI-1943070). The authors acknowledge Dr. Xiao Kuang for providing the SEM image of the NdFeB particles.

References

- Lum, G. Z., Ye, Z., Dong, X., Marvi, H., Erin, O., Hu, W., and Sitti, M., 2016, "Shape-Programmable Magnetic Soft Matter," Proc. Natl. Acad. Sci. U. S. A., 113(41), pp. E6007–E6015.
- [2] Wu, S., Ze, Q., Zhang, R., Hu, N., Cheng, Y., Yang, F., and Zhao, R., 2019, "Symmetry-Breaking Actuation Mechanism for Soft Robotics and Active Metamaterials," ACS Appl. Mater. Interfaces, 11(44), pp. 41649–41658.
- [3] Xu, T., Zhang, J., Salehizadeh, M., Onaizah, O., and Diller, E., 2019, "Millimeter-Scale Flexible Robots With Programmable Three-Dimensional Magnetization and Motions," Sci. Rob., 4(29), p. eaav4494.
- [4] Hu, W., Lum, G. Z., Mastrangeli, M., and Sitti, M., 2018, "Small-Scale Soft-Bodied Robot With Multimodal Locomotion," Nature, 554(7690), pp. 81– 85.
- [5] Ze, Q., Kuang, X., Wu, S., Wong, J., Montgomery, S. M., Zhang, R., Kovitz, J. M., Yang, F., Qi, H. J., and Zhao, R., 2020, "Magnetic Shape Memory Polymers With Integrated Multifunctional Shape Manipulation," Adv. Mater., 32(4), p. 1906657.
- [6] Liu, S., Zhao, Y., Zhao, D., Feng, L., Shi, X., and Chen, L., 2019, "Tunable Band Gap Structures of Acoustic Metamaterials With Magnetorheological Elastomer Cladding Layers," Acta Acust. United Ac., 105(5), pp. 796–804.
- [7] Kim, Y., Yuk, H., Zhao, R., Chester, S. A., and Zhao, X., 2018, "Printing Ferromagnetic Domains for Untethered Fast-Transforming Soft Materials," Nature, 558(7709), pp. 274–279.
- [8] Crivaro, A., Sheridan, R., Frecker, M., Simpson, T. W., and Von Lockette, P., 2016, "Bistable Compliant Mechanism Using Magneto Active Elastomer Actuation," J. Intell. Mater. Syst. Struct., 27(15), pp. 2049–2061.
- [9] Cui, J., Huang, T.-Y., Luo, Z., Testa, P., Gu, H., Chen, X.-Z., Nelson, B. J., and Heyderman, L. J., 2019, "Nanomagnetic Encoding of Shape-Morphing Micromachines," Nature, 575(7781), pp. 164–168.
- [10] Gu, H., Boehler, Q., Ahmed, D., and Nelson, B. J., 2019, "Magnetic Quadrupole Assemblies With Arbitrary Shapes and Magnetizations," Sci. Rob., 4(35), eaax8977.
- [11] Kim, Y., Parada, G. A., Liu, S., and Zhao, X., 2019, "Ferromagnetic Soft Continuum Robots," Sci. Rob., 4(33), p. eaax7329.
- [12] Hellebrekers, T., Kroemer, O., and Majidi, C., 2019, "Soft Magnetic Skin for Continuous Deformation Sensing," Adv. Intell. Syst., 1(4), p. 1900025.
- [13] Jeon, S., Hoshiar, A. K., Kim, K., Lee, S., Kim, E., Lee, S., Kim, J.-y., Nelson, B. J., Cha, H.-J., Yi, B.-J., and Choi, H., 2019, "A Magnetically Controlled Soft Microrobot Steering a Guidewire in a Three-Dimensional Phantom Vascular Network," Soft Rob., 6(1), pp. 54–68.
 [14] Yim, S., and Sitti, M., 2012, "Shape-programmable Soft Capsule
- [14] Yim, S., and Sitti, M., 2012, "Shape-programmable Soft Capsule Robots for Semi-Implantable Drug Delivery," IEEE Trans. Rob., 28(5), pp. 1198–1202.
- [15] Chautems, C., Tonazzini, A., Floreano, D., and Nelson, B. J., "A Variable Stiffness Catheter Controlled with an External Magnetic Field," Proceedings of 2017 IEEE/RSJ International Conference on Intelligent Robots and Systems (IROS), Vancouver, BC, Canada, Sept. 24–28, IEEE, pp. 181–186.
- [16] Miyashita, S., Guitron, S., Yoshida, K., Li, S., Damian, D. D., and Rus, D., "Ingestible, Controllable, and Degradable Origami Robot for Patching Stomach Wounds," Proceedings of 2016 IEEE International Conference on Robotics and Automation (ICRA), Stockholm, Sweden, May 16–21, IEEE, pp. 909–916.
- [17] Bernasconi, R., Cuneo, F., Carrara, E., Chatzipirpiridis, G., Hoop, M., Chen, X., Nelson, B. J., Pané, S., Credi, C., and Levi, M., 2018, "Hard-magnetic Cell Microscaffolds From Electroless Coated 3D Printed Architectures," Mater. Horiz., 5(4), pp. 699–707.
- [18] Erb, R. M., Martin, J. J., Soheilian, R., Pan, C., and Barber, J. R., 2016, "Actuating Soft Matter With Magnetic Torque," Adv. Funct. Mater., 26(22), pp. 3859–3880.
- [19] Zhao, R., Kim, Y., Chester, S. A., Sharma, P., and Zhao, X., 2019, "Mechanics of Hard-Magnetic Soft Materials," J. Mech. Phys. Solids, 124, pp. 244–263.
- [20] Kim, J., Chung, S. E., Choi, S.-E., Lee, H., Kim, J., and Kwon, S., 2011, "Programming Magnetic Anisotropy in Polymeric Microactuators," Nat. Mater., 10(10), pp. 747–752.
- [21] Wu, S., Hamel, C. M., Ze, Q., Yang, F., Qi, H. J., and Zhao, R., 2020, "Evolutionary Algorithm Guided Voxel-Encoding Printing of Functional Hard-Magnetic Soft Active Materials," Advanced Intelligent Systems, p. 2000060.
- [22] Ginder, J., Clark, S., Schlotter, W., and Nichols, M., 2002, "Magnetostrictive Phenomena in Magnetorheological Elastomers," Int. J. Mod. Phys. B, 16(17n18), pp. 2412–2418.
- [23] Kankanala, S., and Triantafyllidis, N., 2004, "On Finitely Strained Magnetorheological Elastomers," J. Mech. Phys. Solids, 52(12), pp. 2869–2908.
- [24] Danas, K., Kankanala, S., and Triantafyllidis, N., 2012, "Experiments and Modeling of Iron-Particle-Filled Magnetorheological Elastomers," J. Mech. Phys. Solids, 60(1), pp. 120–138.
- [25] Han, Y., Mohla, A., Huang, X., Hong, W., and Faidley, L. E., 2015, "Magnetostriction and Field Stiffening of Magneto-Active Elastomers," Int. J. Appl. Mech., 7(1), p. 1550001.
- [26] Lopez-Lopez, M., Durán, J. D., Iskakova, L. Y., and Zubarev, A. Y., 2016, "Mechanics of Magnetopolymer Composites: a Review," J. Nanofluids, 5(4), pp. 479–495.
- [27] Bertotti, G., 1998, Hysteresis in Magnetism: for Physicists, Materials Scientists, and Engineers, Academic Press, San Diego, CA.
- [28] Kalina, K., Brummund, J., Metsch, P., Kästner, M., Borin, D. Y., Linke, J., and Odenbach, S., 2017, "Modeling of Magnetic Hystereses in Soft MREs Filled With NdFeB Particles," Smart Mater. Struct., 26(10), p. 105019.

- [29] Mahdavi, M., Yousefi, E., Baniassadi, M., Karimpour, M., and Baghani, M., 2017, "Effective Thermal and Mechanical Properties of Short Carbon Fiber/ Natural Rubber Composites as a Function of Mechanical Loading," Appl. Therm. Eng., 117, pp. 8–16.
- [30] Wang, W., Dai, Y., Zhang, C., Gao, X., and Zhao, M., 2016, "Micromechanical Modeling of Fiber-Reinforced Composites With Statistically Equivalent Random Fiber Distribution," Materials, 9(8), p. 624.
 [31] Riaño, L., and Joliff, Y., 2019, "An Abaqus™ Plug-in for the Geometry
- [31] Riaño, L., and Joliff, Y., 2019, "An Abaqus[™] Plug-in for the Geometry Generation of Representative Volume Elements With Randomly Distributed Fibers and Interphases," Compos. Struct., 209, pp. 644–651.
 [32] Babu, K., Mohite, P., and Upadhyay, C., 2018, "Development of an RVE and Its
- [32] Babu, K., Mohite, P., and Upadhyay, C., 2018, "Development of an RVE and Its Stiffness Predictions Based on Mathematical Homogenization Theory for Short Fibre Composites," Int. J. Solids Struct., 130, pp. 80–104.
- [33] Tian, W., Qi, L., Zhou, J., Liang, J., and Ma, Y., 2015, "Representative Volume Element for Composites Reinforced by Spatially Randomly Distributed Discontinuous Fibers and Its Applications," Compos. Struct., 131, pp. 366–373.
 [34] Wang, Z., Wang, X., Zhang, J., Liang, W., and Zhou, L., 2011, "Automatic
- [34] Wang, Z., Wang, X., Zhang, J., Liang, W., and Zhou, L., 2011, "Automatic Generation of Random Distribution of Fibers in Long-Fiber-Reinforced Composites and Mesomechanical Simulation," Mater. Des., 32(2), pp. 885–891.
- [35] Yang, W., Gao, Z., Yue, Z., Li, X., and Xu, B., 2019, "Hard-Particle Rotation Enabled Soft-Hard Integrated Auxetic Mechanical Metamaterials," Proc. R. Soc. A, 475(2228), p. 20190234.

- [36] Zhang, H., Yang, W., and Xu, B., 2019, "Rotation Mechanics of Optical Scatters in Stretchable Metasurfaces," Int. J. Solids Struct., 191–192, pp. 566– 576
- [37] Aryanto, D., Ray, Z., Sudiro, T., Wismogroho, A. S., and Sudrajat, N., 2015, "The Effect of Powder Particle Size on the Structural and Magnetic Properties of Bonded NdFeB Magnet," Adv. Mater. Res, 1123, pp. 88–91.
- [38] Huang, Y., Liu, Z., Zhong, X., Yu, H., and Zeng, D., 2012, "NdFeB Based Magnets Prepared From Nanocrystalline Powders With Various Compositions and Particle Sizes by Spark Plasma Sintering," Powder Metall., 55(2), pp. 124– 129.
- [39] Wang, Y., Hu, Y., Chen, L., Gong, X., Jiang, W., Zhang, P., and Chen, Z., 2006, "Effects of Rubber/Magnetic Particle Interactions on the Performance of Magnetorheological Elastomers," Polym. Test., 25(2), pp. 262– 267.
- [40] Wells, J., Löwa, N., Paysen, H., Steinhoff, U., and Wiekhorst, F., 2019, "Probing Particle-Matrix Interactions During Magnetic Particle Spectroscopy," J. Magn. Magn. Mater., 475, pp. 421–428.
- [41] Osman, M. A., and Atallah, A., 2005, "Interparticle and Particle-Matrix Interactions in Polyethylene Reinforcement and Viscoelasticity," Polymer, 46(22), pp. 9476–9488.
- [42] Yang, W., Liu, Q., Yue, Z., Li, X., and Xu, B., 2017, "Rotation of Hard Particles in a Soft Matrix," J. Mech. Phys. Solids, 101, pp. 285–310.